The high-rate brittle microplane concrete model: Part II: application to projectile perforation of concrete slabs

Andreas O. Frank, Mark D. Adley*, Kent T. Danielson and Henry S. McDevitt, Jr.

*U.S. Army Engineer Research and Development Center Impact and
Explosive Effects Branch, ATTN: CEERD-GM-I 3909
Halls Ferry Road Vicksburg, MS 39180-6199 USA*

Abstract. In this paper, we examine the behavior of the High-Rate Brittle Microplane (HRBM) concrete model based on a series of penetration experiments. These experiments were conducted with three different slab thicknesses (127, 216 and 254 mm) that provided a significant challenge for the numerical simulations. The 127 mm slab provided little resistance, the 216 mm slab provided nominal resistance and the 254 mm slab approached the perforation limit thickness of the projectile. These experiments provide a good baseline for evaluating material models since they have been shown to be extremely challenging; in fact, we have not encountered many material models that can provide quantitatively predictive results in terms of both projectile exit velocity and material damage. In a companion paper, we described the HRBM material model and its fit to various quasi-static material property data for WES-5000 concrete. In this paper, we show that, when adequately fit to these quasi-static data, the HRBM model does not have significant predictive capabilities, even though the quasi-static material fit may be exceptional. This was attributed to the rate-dependent response of the material. After various rate effects were introduced into the HRBM model, the quantitative predictive nature of the calculations dramatically increased. Unfortunately, not much rate-dependent material property data are in the literature; hence, accurate incorporation of rate effects into material models is difficult. Nonetheless, it seems that rate effects may be critical in obtaining an accurate response for concrete during projectile perforation events.

Keywords: numerical modeling; strain-rate dependence; microplane models.

1. Introduction

The Geotechnical and Structures Laboratory of the U.S. Army Engineer Research and Development Center (ERDC) has conducted a significant amount of projectile penetration research. These efforts included numerous projectile penetration experiments using the ERDC 83 mm ballistic research facility (Frew *et al.* 1993), extensive material property experiments that characterize target mechanical property behavior and provide data for fitting constitutive models (Akers *et al.* 1995) and numerous first-principle calculations of various penetration events (Adley *et al.* 2010). Our research is focused on gathering data and gaining insight into the processes of penetration mechanics. One of the end goals of our research is to develop more accurate and robust material models.

In this paper, we examine the behavior of the High-Rate Brittle Microplane (HRBM) concrete

---

* Corresponding author, Ph.D., E-mail: mark.d.adley@usace.army.mil

model during various projectile perforation events. A series of penetration experiments into conventional strength concrete (WES-5000) were conducted at ERDC using ogive-nose projectiles weighing about 2.3 kilograms (Cargile 1999). The projectiles were launched at conventional velocities into three unreinforced concrete slabs having thicknesses of 127, 216, and 254 mm. The experiments offer a challenge to the numerical simulations by providing three distinctly different target responses as follows: a relatively thin slab providing little resistance, an intermediate slab providing nominal resistance, and a relatively thick slab approaching the perforation limit thickness for the projectile. These experiments provide a good baseline for evaluating material models since they have been shown to be extremely challenging. In fact, we have not encountered many material models that can provide quantitatively predictive results in terms of both projectile exit velocity and material damage.

Projectile perforation events typically produce high-pressures over a small region under the nose of the projectile as it penetrates the target. However, the majority of the target's response is dominated by the low-pressure "brittle" behavior of concrete (Frank and Adley 2007). More specifically, the formation of the impact and exit craters are typically dominated by low confinement stress states under compression, extension and/or tension within the target material. Furthermore, it is imperative to accurately capture the "brittle" or "softening" behavior of the material. Fig. 1 shows the "softening" behavior of low-pressure triaxial material property data, as well as the resulting "shear bands" that arise in a perforation calculation due to the material's "softening" response. Notice that accurate modeling of the material softening behavior is required to adequately predict both the material damage, i.e., impact and exit craters and projectile exit velocity.

In a companion paper, we described the HRBM material model and its fit to various quasi-static material property data for WES-5000 concrete (Adley *et al.* 2010). In this paper, we show that when adequately fit to these quasi-static data, the HRBM model does not have significant quantitatively predictive capabilities, even though the quasi-static material fit may be exceptional. This observation is not necessarily surprising and is attributed to the rate-dependent response of the material. Furthermore, once the appropriate rate effects were introduced into the HRBM model, the quantitative predictive nature of the calculations dramatically increased. Unfortunately, there is not much rate-dependent material property data in the literature and none available for WES-5000 concrete. Hence, accurate incorporation of the rate effects into the HRBM model is difficult. Nonetheless, it seems that rate effects may be critical in obtaining an accurate response for concrete during projectile perforation events.

(a)   (b)
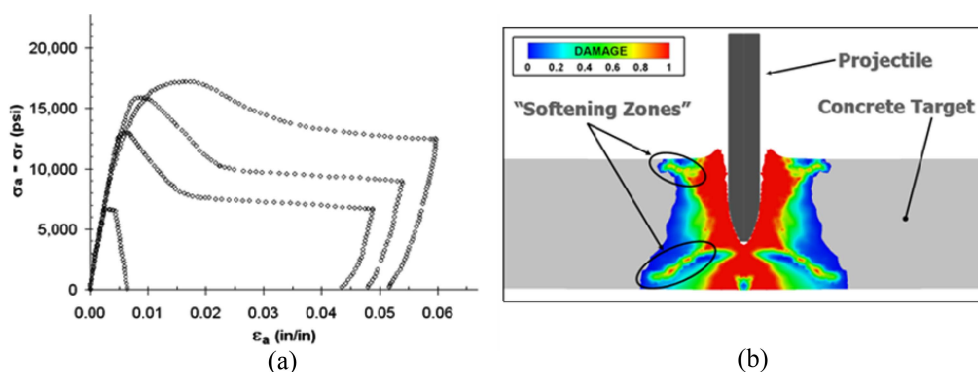
Fig. 1   The material "softening" response observed in concrete, (a) Post-peak softening from stress versus strain TXC lab data at low pressures (<20 MPA), (b) Localized "shear bands" or "softening zones" that develop during a projectile perforation event due to the material softening response (Frank and Adley 2007)

2. High-rate brittle microplane model and material fit

2.1 Model description

The HRBM model uses the M4 microplane model (Bazant *et al*. 2000, Caner and Bazant 2000) as its foundation. The M4 model typically provides very reasonable results for the target damage caused by projectile penetration, embedded detonation and blast-related problems (Danielson *et al*. 2010, Littlefield *et al*. 2010). The HRBM model introduces additional bounding curves into the M4 model framework that were designed to more accurately capture the hydrostatic behavior of concrete as
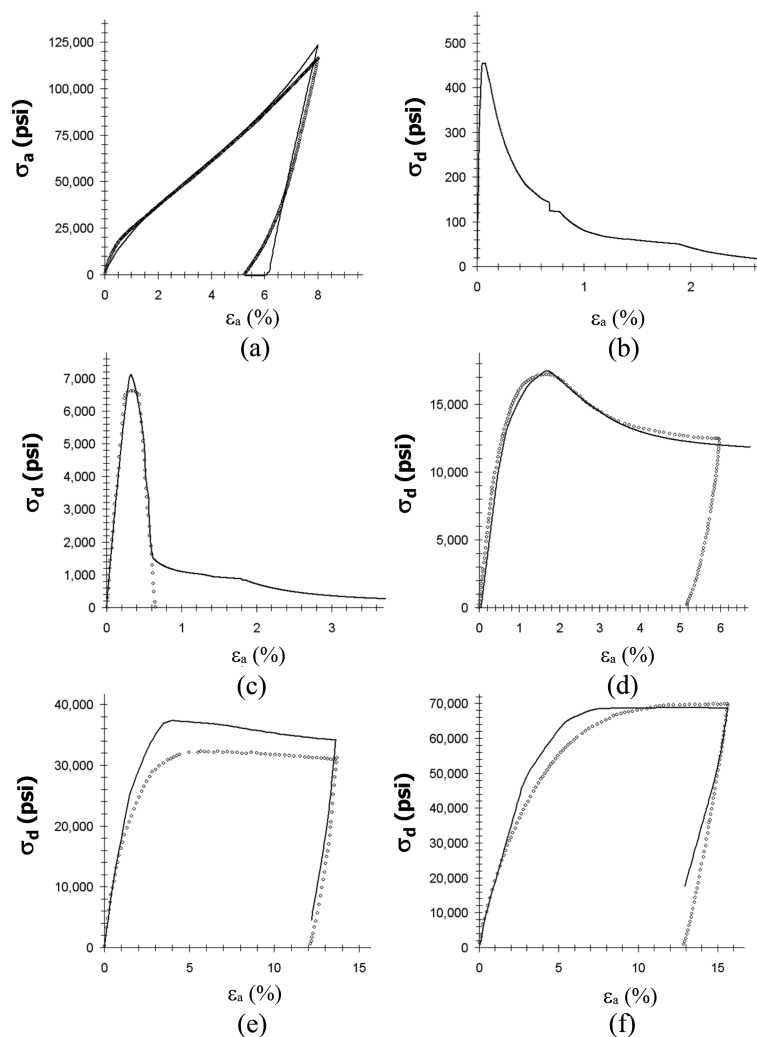
Fig. 2   The HRBM model fit to quasi-static lab data for WES-5000 concrete. The model response is shown as solid lines and the lab data as discrete circles, (a) axial stress versus axial strain for uniaxial compression, (b) principal stress difference versus axial strain for direct pull, (c) principal stress difference versus axial strain for unconfined compression and principal stress difference versus axial strain for triaxial compression, (d) at 20 MPa, (e) at 100 MPa and (f) at 400 MPa

well as its low-pressure triaxial behavior and transition to high-pressure behavior. This provides a greatly increased resolution in fitting the quasi-static material property data. The HRBM model is described in greater detail in a companion paper (Adley *et al.* 2010).

2.2 Quasi-static material fit

We fit the HRBM model to a conventional strength concrete mix developed at ERDC and known as WES-5000 concrete (Cargile 1999). It is our experience that the material fitting of the HRBM model requires the use of an automated fitting code. Further details on the material fitting procedure are described in a companion paper (Adley *et al.* 2010). Fig. 2 shows a sample from the material fit of the HRBM model to WES-5000 concrete. Shown are the material responses in uniaxial strain, unconfined tension, unconfined compression, 20 MPa triaxial compression, 100 MPa triaxial compression and 400 MPa triaxial compression. Notice the exceptional comparative responses for the uniaxial strain as well as the low-pressure triaxial compression. It should also be noted that the HRBM model provides an increased level of flexibility that will be required to fit emerging high-strength concrete materials that contain glass (Roth e*t al.* 2010) and steel fibers (Williams *et al.* 2010).

3. Hydrocode perforation calculations

3.1 Perforation experiments

A series of penetration experiments into WES-5000 concrete were conducted at ERDC (Cargile 1999). The penetrators used in these experiments were 2.3 kg ogival nose projectiles (caliber radius head = 3.0, length/diameter ratio = 7.0 and diameter = 50.8 mm). The projectiles were launched into three unreinforced concrete slabs with thicknesses of 127, 216 and 254 mm. Each slab was constructed in a steel culvert with a nominal diameter of 1,520 mm, providing a nearly semi-infinite width. For example, the target width to projectile diameter ratio, or W/D, for these experiments was more than 30. All the experiments were conducted under "near" normal impact conditions. The angle-of-obliquity and angle-of-attack were less than 1 degree with an impact velocity of approximately 310 m/s. All of the experiments resulted in complete perforation of the concrete slabs. Fig. 3 shows representative results from these experiments. Shown in this figure are the projectile exit velocities
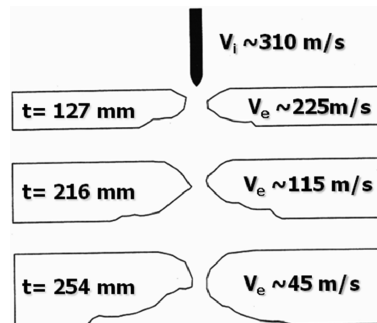

Fig. 3 Representative results from perforation experiments (Cargile 1999). Shown are the impact (V_i) and exit (V_e) velocities, as well as the final crater shapes

and the measured posttest concrete damage in terms of the final impact and exit crater profiles. We will evaluate the HRBM model against these experimental penetration data by conducting numerical simulations using the EPIC hydrocode (Johnson *et al.* 2008).

3.2 Perforation calculations using quasi-static material fit

We conducted 2D axi-symmetric EPIC simulations of the perforation experiments discussed above using the HRBM model and its fit to WES-5000 quasi-static concrete material property data. Our finite element models, composed of linear triangular elements, were developed to focus on the target response. Hence, we provided a relatively low fidelity for the projectile and a higher fidelity for each of the target slabs. For example, each target slab had a characteristic element size near the point of impact that was approximately 5 mm. This provided a target resolution of about 10 elements per projectile diameter, i.e., 50.8 mm. All calculations were conducted using the element-
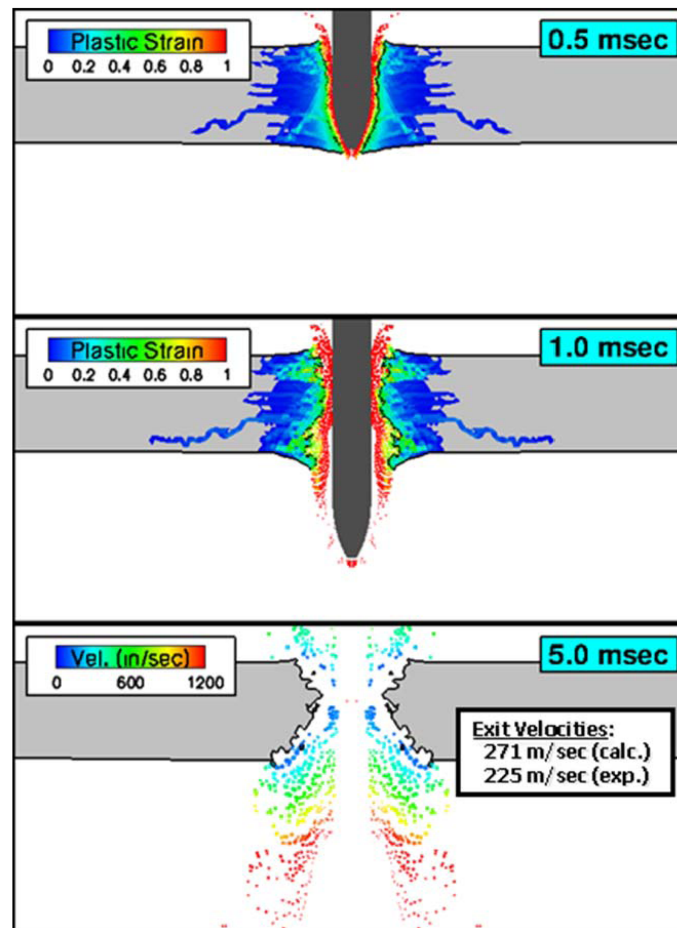

Fig. 4 A hydrocode calculation of a projectile perforating a 127 mm-thick concrete slab using the HRBM model. Shown are effective plastic strain contours at 0.5 and 1.0 msec along with the projectile exit velocities, i.e., both calculated and experimental. Also shown are material velocities at 5.0 msec, which provide an indication of the residual damage in terms of impact and exit crater shapes

to-particle conversion algorithms in the EPIC hydrocode (Johnson *et al.* 2008). Various other methods for treating element failure were considered but will not be discussed in this paper.

The slideline defined between the projectile and target models was frictionless, i.e., the coefficient of friction was set to zero. Further details on the numerical algorithms employed in the EPIC finite element code can be found in the EPIC manual (Johnson *et al.* 2008). Finally, a simple regularization procedure is integrated into the artificial viscosity algorithm used in EPIC to mitigate mesh sensitivity concerns (Frank 2011). The aforementioned procedure separates the regularization algorithm from the constitutive model and the fitting process(optimization algorithm).

In order to evaluate our calculations, we used the experimentally determined projectile exit velocities and the final crater profiles from Fig. 3 as the "gold standard". Specifically, the exit velocities provide a global measure of the penetration resistance, whereas the final crater shapes provide a global measure of the residual concrete damage. Figs. 4 through 6 show snapshots of effective plastic strain and material velocities taken from the EPIC simulations. Notice that the
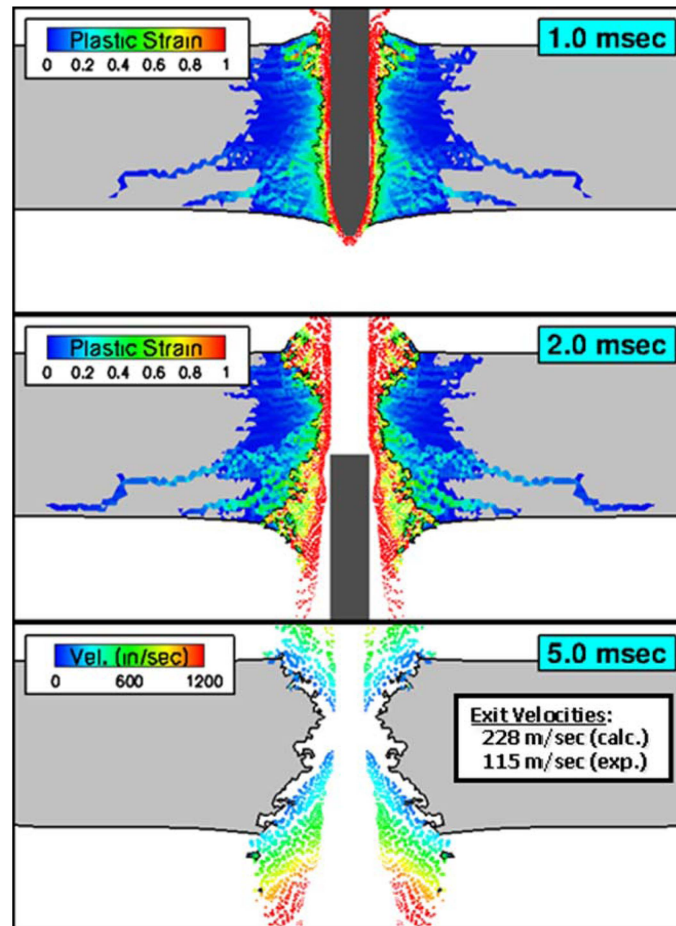

Fig. 5   A hydrocode calculation of a projectile perforating a 216 mm-thick concrete slab using the HRBM model. Shown are effective plastic strain contours at 1.0 and 2.0 msec along with the projectile exit velocities, i.e., both calculated and experimental. Also shown are material velocities at 5.0 msec, which provide an indication of the residual damage in terms of impact and exit crater shapes
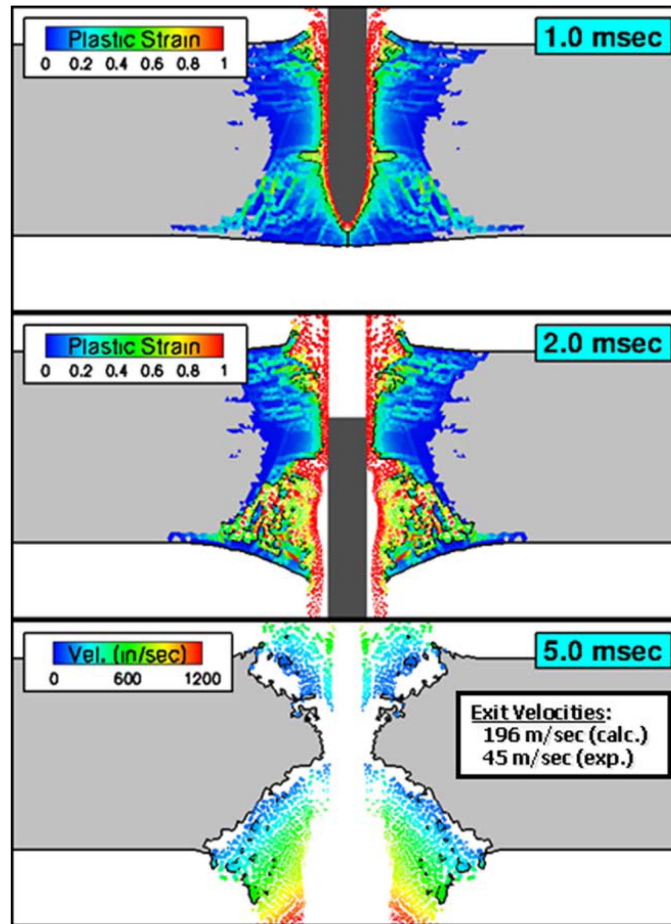
Fig. 6 A hydrocode calculation of a projectile perforating a 254 mm-thick concrete slab using the HRBM model. Shown are effective plastic strain contours at 1.0 and 2.0 msec along with the projectile exit velocities, i.e., both calculated and experimental. Also shown are material velocities at 5.0 msec, which provide an indication of the residual damage in terms of impact and exit crater shapes

plastic strain snapshots show the early formation of the impact and exit craters, whereas the material velocity snapshot shows the final crater shapes. Fig. 4 shows the 127 mm-thick slab at 0.5, 1.0 and 5.0 msec, Fig. 5 shows the 216 mm-thick slab at 1.0, 2.0 and 5.0 msec, and Fig. 6 shows the 254 mm-thick slab at 1.0, 2.0 and 5.0 msec. Also shown in these figures are the calculated projectile exit velocities. Notice that, for all three slabs, the exit velocities are significantly overestimated. For example, there is a +20%, +98% and +336% error for the 127-, 216- and 254 mm slabs, respectively. Furthermore, as the slab thickness increases, the overestimation of the exit velocity also significantly increases. This highlights the extreme difficulty most material models seem to show when predicting penetration events near the perforation limit thickness of the projectile, i.e., similar to the 254 mm-thick slab. It should be emphasized that, although the HRBM model was able to provide an exceptional fit to the quasi-static material property data (see Fig. 2), the quantitative predictive capability during these perforation events was not very good. We believe the reason for this is due to the rate-dependent behavior of the material, which was included in the material model.

4. Discussion

4.1 Rate-dependent bounding curves

Although the HRBM model produced an exceptional material response under well-controlled quasi-static laboratory stress states (see Fig. 2), the material behavior during projectile perforation events was not acceptable. The reason for this lies in the rate-dependent behavior of the material. For example, concrete can have increased strength at higher strain rates (Schuler *et al.* 2003, Frew 2001, Luk *et al*. 2007). It is also known that the strength of concrete is pressure dependent. However, without adequate material property data, it can be difficult to describe the behavior of concrete as a function of both rate and pressure. Nonetheless, we believe that data suggests that the rate effects are more dominant at lower pressures. For example, unconfined tensile tests usually show very strong rate dependence (Schuler *et al.* 2003), whereas unconfined compression tests show weaker rate dependence (Frew 2001). Furthermore, recent higher pressure Hopkinson bar data may also suggest that the rate effects decrease as the pressure increases (Luk *et al.* 2007). We hypothesized that damage must be a rate-dependent process, i.e., void crushing, spreading, splitting, micro-crack formation, crack growth and crack coalescence. Thereby, the rate effects should be introduced into only these mechanisms. For example, perhaps the strength-dependent rate effects are dominated by the cohesive strength of the material and not the frictional strength. In fact, perhaps the frictional strength for concrete shows some velocity weakening as seen in geomaterials under earthquake-type loadings (Niemeijer and Spiers 2007, Di Toro *et al.* 2004). Furthermore, recent pressurized Hopkinson bar data for fine sand, i.e., a pure frictional material without cohesion, showed negligible strength-dependent rate effects (Kabir *et al.* 2010). It should be noted that this is contrary to many material models, which typically apply the strength-dependent rate effects to the frictional strength response of the material, i.e., high pressures and/or Mises limit. Fig. 7 provides a schematic representation of both the frictional and cohesive parts of the material strength. It is our hypothesis that the rate effects should be predominantly acting on the cohesive part of the material strength.

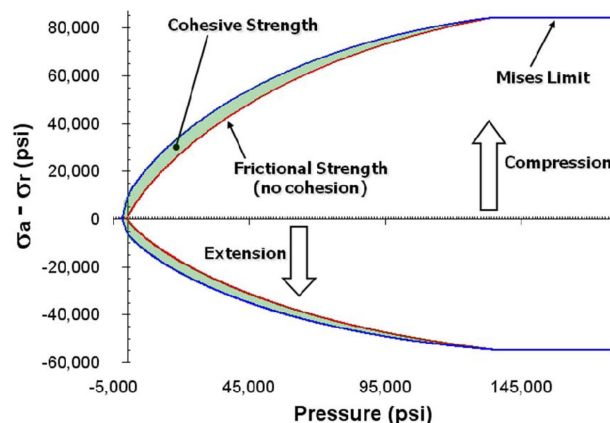We introduced rate effects into the HRBM model by individually scaling each of the boundary

Fig. 7 A hypothetical failure envelope for concrete. Shown are representations for the cohesive and frictional strength in both compression and extension

curves (Adley *et al.* 2010) according to a rate amplification factor (χ_i^{rate}), as follows

$$\chi_i^{rate} = \dot{\varepsilon}_{norm}^{C_i} \qquad \dot{\varepsilon}_{norm} = \max\left(\frac{\dot{\varepsilon}}{\dot{\varepsilon}_{quasi-static}}, 1.0\right) \qquad (1)$$

where $\dot{\varepsilon}_{norm}$ is the normalized strain rate, $\dot{\varepsilon}$ is the actual strain rate, $\dot{\varepsilon}_{quasi-static}$ is the quasi-static strain rate and C_i are the rate constants for each individual bounding curve. The actual strain rate is computed by dividing the increment of the effective strain by the time increment. For example, each set of bounding curves (volumetric, frictional, deviatoric and normal) has a separate rate amplification factor (χ_i^{rate}) based on its rate constant (C_i). Due to the lack of available lab data, we were not able to calibrate the HRBM model rate effects very rigorously using well-controlled laboratory material property data. Therefore, we calibrated the numeric values of the rate constants (C_i) based on the penetration experiments discussed above. This led to very strong rate effects on the deviatoric and tensile normal bounding curves, since they are responsible for the cohesive strength of the material. Furthermore, only mild rate effects were applied to the frictional and volumetric bounding curves.

Figs. 8 through 11 show the rate effects for the HRBM bounding curves as fitted to WES-5000 concrete. Shown are the bounding curves for a quasi-static strain rate (10^{-4} sec^{-1}), as well as various higher strain rates. The typical strain rates observed during the perforation events of interest are approximately 10^3 sec^{-1}. Fig. 8 shows the compressive volumetric boundary and Fig. 9 shows the frictional yield boundary for both quasi-static and a strain rate of 10^3 sec^{-1}. Fig. 10 shows the deviatoric boundaries and Fig. 11 shows the tensile normal boundary for quasi-static and strain rates of 10^1, 10^2 and 10^3 sec^{-1}. Notice that the rate effects we have considered are more dominant for the
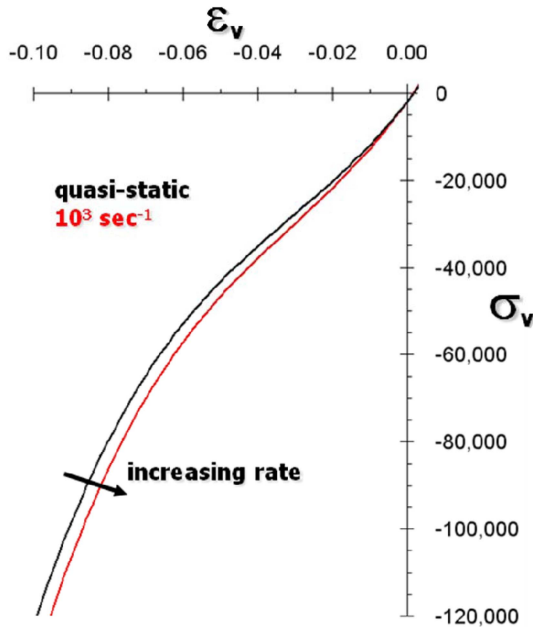

Fig. 8   The quasi-static compressive volumetric boundary along with a high-rate boundary representative of the perforation events of interest (10^3 sec^{-1})
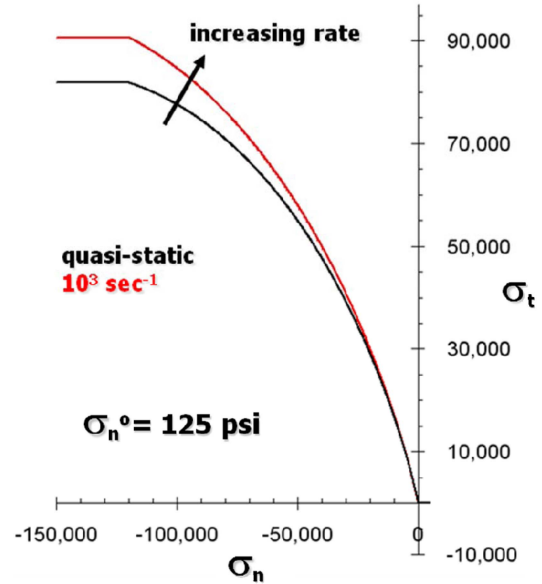
Fig. 9   The quasi-static frictional shear boundary along with a high-rate boundary representative of the perforation events of interest (10^3 sec^{-1})
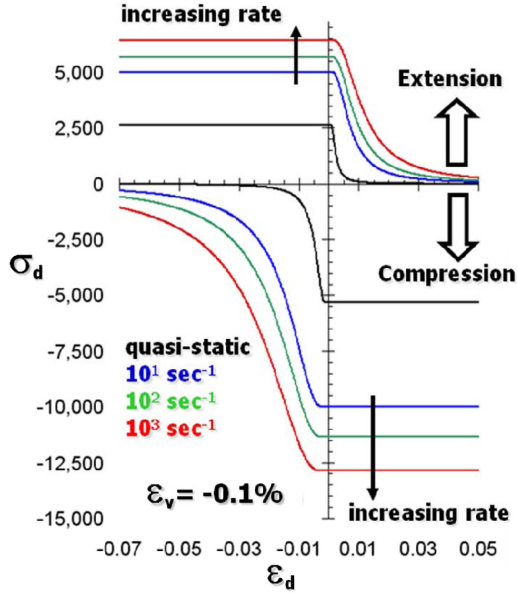
Fig. 10 The quasi-static deviatoric boundaries (compression and extension) along with various higher rate boundaries (10^1, 10^2 and 10^3 sec^{-1})
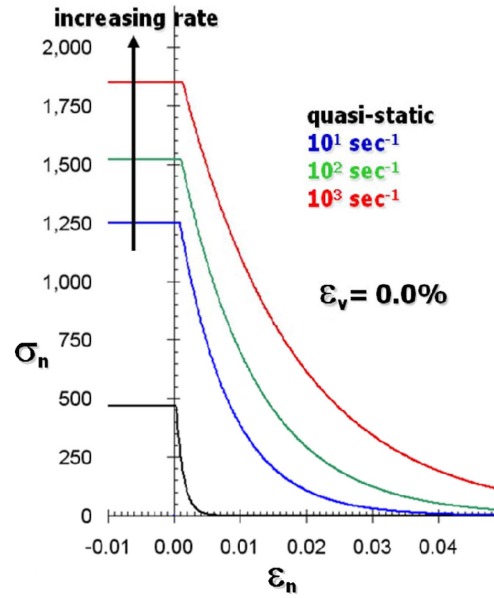
Fig. 11 The quasi-static tensile normal stress boundary along with various higher rate boundaries (10^1, 10^2 and 10^3 sec^{-1})
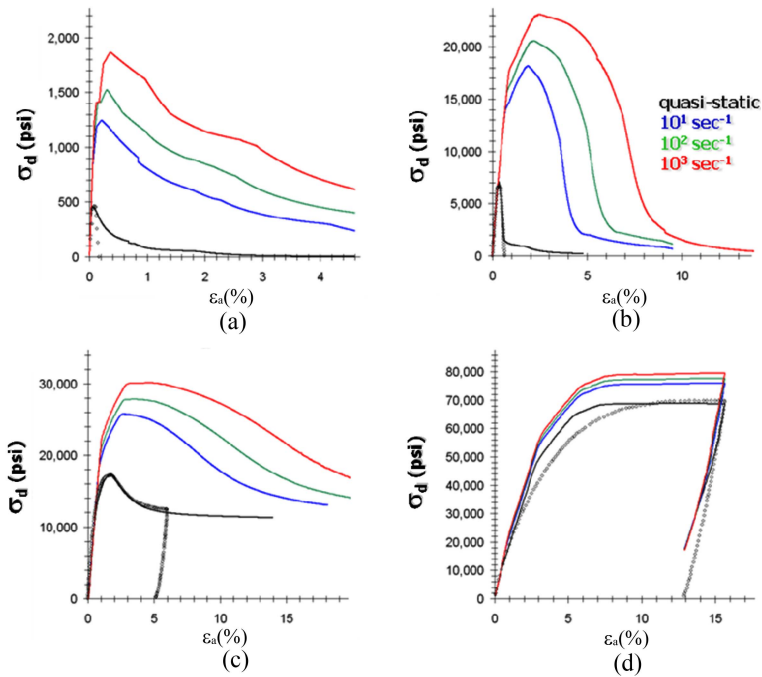

Fig. 12 Influence of the rate effects for the HRBM model fit to WES-5000 concrete, i.e., quasi-static, 10^1 sec^{-1}, 10^2 sec^{-1} and 10^3 sec^{-1}, (a) principal stress difference versus axial strain for direct pull, (b) principal stress difference versus axial strain for unconfined compression and principal stress difference versus axial strain for triaxial compression, (c) at 20 MPa and (d) at 400 MPa. Also shown are the quasi-static lab data as discrete circles

cohesive boundaries, i.e., deviatoric and tensile normal. Fig. 12 shows the high-rate response (10^3 sec^{-1}) using a material driver code (Adley *et al.* 2010) for simulating the unconfined tension, unconfined compression, 20 MPa triaxial compression and 400 MPa triaxial compression stress paths. Notice that the rate effects are more dominant at lower confining pressures, i.e., unconfined.

4.2 Perforation calculations with rate-dependent bounding curves

Using the HRBM model along with the rate effects described above, we repeated the hydrocode simulations for projectile perforations of the 127-, 216- and 254 mm WES-5000 concrete slabs. Figs. 13 through 15 show the transient results from the HRBM model with the inclusion of rate effects for each of the aforementioned slab thicknesses. Each figure shows three snapshots in time during the perforation events, i.e., two early-time snapshots as the projectile is within the target and
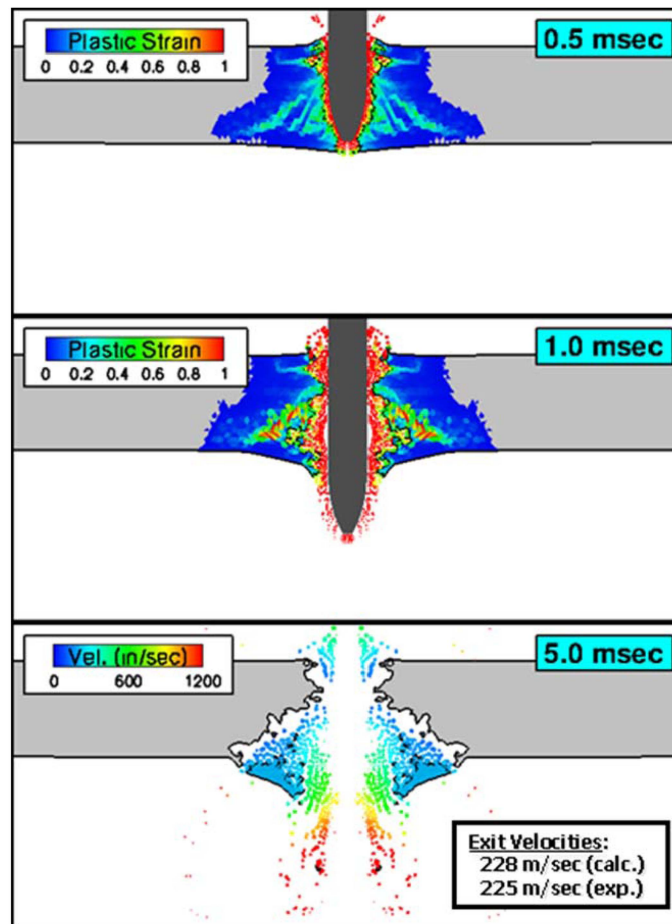

Fig. 13 A hydrocode calculation of a projectile perforating a 127 mm-thick concrete slab using the HRBM model with rate effects. Shown are effective plastic strain contours at 0.5 and 1.0 msec along with the projectile exit velocities, i.e., both calculated and experimental. Also shown are material velocities at 5.0 msec, which provide an indication of the residual damage in terms of impact and exit crater shapes
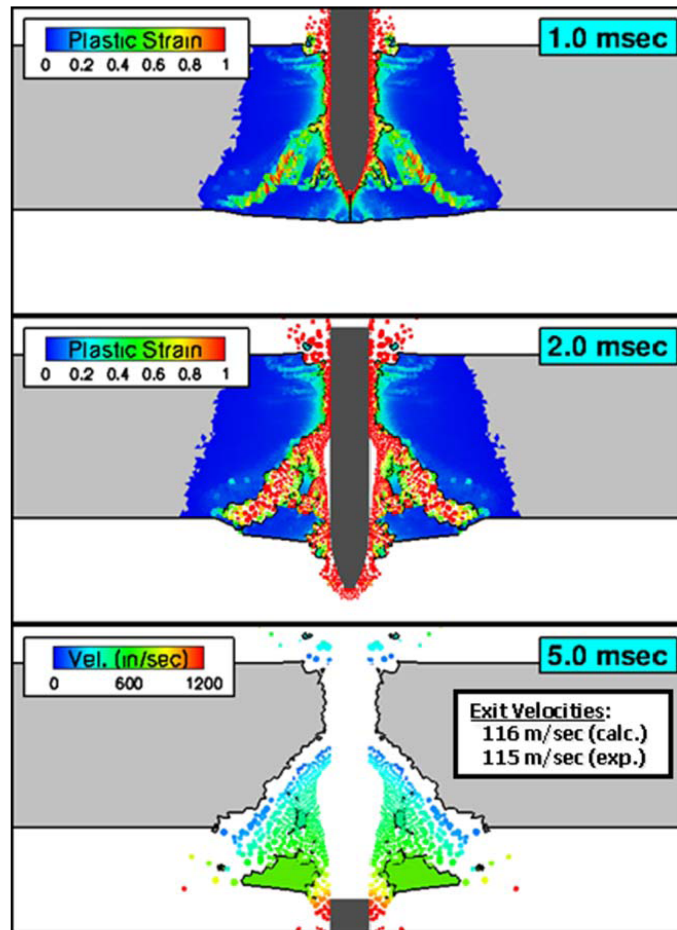
Fig. 14 A hydrocode calculation of a projectile perforating a 216 mm-thick concrete slab using the HRBM model with rate effects. Shown are effective plastic strain contours at 1.0 and 2.0 msec along with the projectile exit velocities, i.e., both calculated and experimental. Also shown are material velocities at 5.0 msec, which provide an indication of the residual damage in terms of impact and exit crater shapes

one late-time snapshot as the impact and exit craters have sufficiently formed. Fig. 13 shows the hydrocode results for the 127 mm-thick slab at 0.5, 1.0 and 5.0 msec. Fig. 14 shows the hydrocode results for the 216 mm-thick slab at 1.0, 2.0 and 5.0 msec. Fig. 15 shows the hydrocode results for the 254 mm-thick slab at 1.0, 2.0 and 5.0 msec. Notice that for each hydrocode simulation, the projectile penetration resistance significantly increased compared to the calculations that do not include rate effects, i.e., Figs. 4, 5 and 6. Furthermore, the quantitative predictive capability of these calculations seems to be much improved when using rate effects. For example, now there is only a +1%, +1% and -29% error for the 127-, 216- and 254 mm slabs, respectively. Also notice that the damage craters are more distinctly formed when using the rate effects, i.e., more distinct shear bands or softening zones.
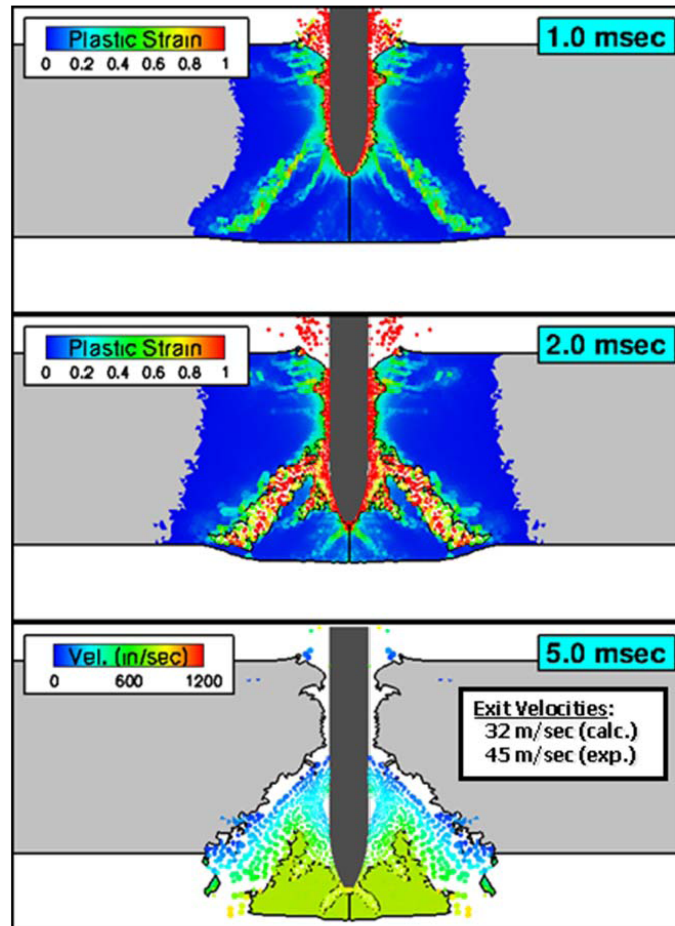
Fig. 15 A hydrocode calculation of a projectile perforating a 254 mm-thick concrete slab using the HRBM model with rate effects. Shown are effective plastic strain contours at 1.0 and 2.0 msec along with the projectile exit velocities, i.e., both calculated and experimental. Also shown are material velocities at 5.0 msec, which provide an indication of the residual damage in terms of impact and exit crater shapes

5. Conclusions

We fit the HRBM concrete model to various quasi-static material property data for WES-5000 concrete with exceptional results. We then conducted hydrocode calculations of various projectile perforation events. Although the quasi-static material fit seemed to be exceptional, the quantitative predictive nature of these calculations was not very good. Specifically, the projectile exit velocities were greatly overestimated, especially for the thicker slabs. We then introduced rate effects into the HRBM concrete model. Since no specific rate-dependent material property data were available for WES-5000 concrete, we hypothesized that the rate effects should be more dominant on the cohesive material strength and not the frictional strength. We then calibrated the magnitude for each rate effect using the perforation experiments described herein. It was observed that the HRBM model

behaved significantly better once these rate effects were included. This suggests the vital importance that accurate rate effects may play in predicting projectile perforation events.

Acknowledgements

References

Adley, M.D., Frank, A.O. and Danielson, K.T. (2010), "The high-rate brittle microplane concrete model: Part I: bounding curves and quasi-static fit to material property data", *Comput. Concrete*.

Adley, M.D., Frank, A.O., Danielson, K.T., Akers, S.A. and O'Daniel, J.L. (2010), "The virtual penetration laboratory: new developments for projectile penetration in concrete", *Comput. Concrete*, **7**(2), 87-102.

Akers, S.A., Adley, M.D. and Cargile, J.D. (1995), "Comparison of constitutive models for geologic materials used in penetration and ground shock calculations", Proceedings of the 7th International Symposium on the Interaction of Conventional Munitions with Protective Structures, Mannheim FRG.

Bazant, Z.P., Caner, F.C., Carol, I., Adley, M.D. and Akers, S.A. (2000), "Microplane model M4 for concrete, I: formulation with work-conjugate deviatoric stress", *J. Eng. Mech.-ASCE*, **126**(9), 944-953.

Caner, F.C. and Bazant, Z.P. (2000), "Microplane model M4 for concrete. II: algorithm and calibration", *J. Eng. Mech.-ASCE*, **126**(9), 954-961.

Cargile, J.D. (1999), "Development of a constitutive model for numerical simulations of projectile penetration into brittle geomaterials", Technical Report SL-99-11, U.S. Army Engineer Research and Development Center, Vicksburg, MS.

Danielson, K.T., Adley, M.D. and O'Daniel, J.L. (2010), "Numerical procedures for extreme impulsive loading on high strength concrete structures", *Comput. Concrete*, **7**(2), 159-167.

Di Toro, G.D., Goldbsy, D.L. and Tullis, T.E. (2004), "Friction falls towards zero in quartz rock as slip velocity approaches seismic rates", *Nature*, **427**(6973), 436-439.

Frank, A.O. (2011), "An elastic-plastic material model for concrete under high-rate impulsive loads: modeling, implementation, and testing of the high-rate-brittle (HRB) concrete model", GSL-ERDC Tech. Report, draft.

Frank, A.O. and Adley, M.D. (2007), "On the importance of a three-invariant model for simulating the perforation of concrete slabs", Proceedings of the 78th Shock and Vibration Symposium, Philadelphia, PA, 4-8.

Frew, D.J. (2001), "Dynamic response of brittle materials from penetration and split hopkinson pressure bar experiments", Technical Report ERDC/GSL TR-01-6, U.S. Army Engineer Research and Development Center, Vicksburg, MS.

Frew, D.J., Cargile, J.D. and Ehrgott, J.Q. (1993), "WES geodynamics and projectile penetration research facilities", Proceedings of the Symposium on Advances in Numerical Simulation Techniques for Penetration and Perforation of Solids, 1993 ASME Winter Annual Meeting, New Orleans, LA.

Johnson, G.R., Beissel, S.R., Gerlach, C.A., Stryk, R.A. and Holmquis, T.J. (2008), "User instructions for the 2009 beta version of the EPIC code", Southwest Research Institute, San Antonio, TX.

Kabir, M.E., Song, B., Martin, B.E. and Chen, W. (2010), "Compressive behavior of fine sand", Sandia National Laboratories Technical Report SAND2010-2289, Sandia National Laboratories, Albuquerque, NM.

Littlefield, D., Walls, K.C. and Danielson, K.T. (2010), "Integration of the microplane constitutive model into the EPIC code", *Comput. Concrete*, **7**(2), 145-158.

Luk, V.K., Fossum, A.F., Craft, D.C., Fortier, A.E., Cargile, J.D., Averett, J.G. and Williams, E.M. (2007), "Dynamic characterization and penetration analysis of fine aggregate cementitious material", Proceedings of the 12th International Symposium on Interaction of the Effects of Munitions with Structures, New Orleans,

LA.

Niemeijer, A.R. and Spiers, C.J. (2007), "A microphysical model for strong velocity weakening in phyllosilicate-bearing fault gouges", *J. Geophys. Res.*, **112**(10), 1-12.

Roth, J.M., Slawson, T.R. and Flores, O.G. (2010), "Flexural and tensile properties of a glass fiber-reinforced ultra-high-strength concrete: an experimental, micromechanical and numerical study", *Comput. Concrete,* **7**(2), 169-190.

Schuler, H., Mayrhofer, C. and Thoma, K. (2003), "Experimental determination of damage parameter and implementation into a new damage law", Proceedings of the 11th International Symposium on Interaction of the Effects of Munitions with Structures, Mannheim, GE.

Williams, E.M., Graham, S.S., Akers, S.A., Reed, P.A. and Rushing, T.S. (2010), "Constitutive property behavior of an ultra-high-performance concrete with and without steel fibers", *Comput. Concrete*, **7**(2), 191-202.

CC